Effects of Y substitution on the electronic structure and charge dynamics of SmS

Y. Yokoyama,[1,*] H. Hasegawa,[1] Y. Mizuno,[1] D. Asai,[1] Y. Okamoto,[1] H. S. Suzuki,[2] K. Takehana,[3] Y. Imanaka,[3] and K. Takenaka[1]

[1]*Department of Applied Physics, Nagoya University, Furo-cho, Chikusa-ku, Nagoya 464-8603, Japan*
[2]*The Institute for Solid State Physics, The University of Tokyo, Kashiwanoha, Kashiwa 277-8581, Japan*
[3]*National Institute for Materials Science (NIMS), Sakura, Tsukuba 305-0003, Japan*

(Received 5 July 2019; revised manuscript received 14 October 2019; published 24 December 2019)

Evolution of the electronic state by Y doping was explored by optical conductivity covering a wide energy and compositional region deduced from systematic reflectivity measurements of $Sm_{1-x}Y_xS$ single crystals. Although electrons doped onto the 5*d* band by Y dopants immediately realize a metallic state, the charge dynamics do not obey a simple Drude response and the spectral intensity is condensed in the mid-infrared region. Contrary to the pressure-induced case, a metallic phase appears in a certain compositional region before reaching the valence transition. The Fermi level is shifted upwards by electron doping. Therefore, the 5*d* band must overlap with the weakly dispersive 4*f* band more deeply than in the pressure-induced case to reach the valence transition, which can explain the stability of the divalent phase up to higher temperatures in the doped system than in the pressure-induced case. The present optical study provides us with a strategy that sulfur deficiency might increase operating temperature of negative thermal expansion in this system.

DOI: 10.1103/PhysRevB.100.245143

I. INTRODUCTION

Valence transition has long fascinated researchers as a remarkable phenomenon exhibited by rare earth compounds [1,2]. Among them, samarium compounds [3,4] have attracted many researchers to date because of relatively large valence change and various physical properties associated with it. In particular, numerous studies have been reported about samarium monosulfide (SmS) [5–13]. The valence transition of SmS is induced by various stimuli such as pressure and chemical doping. It is accompanied by drastic changes in physical properties including huge volume change up to 10% as well as vivid change of color from black to gold. Attention has recently been drawn from the physics of an excitonic insulator [14,15] and also from the function of giant isotropic negative thermal expansion (NTE) originating from volume change because of the valence transition [16–19].

Valence transition is regarded as triggered by lowering of the 5*d* conduction band to the weakly dispersive 4*f* valence band by pressure or electron doping [3] and the processes of valence transition with pressure and chemical doping might be different. How such differences in the valence-transition process affect macroscopic physical properties is not only important to understanding the phenomena but also useful for improving the NTE function. In the field of NTE, a strategy for improving the material function in terms of the electronic structure has been strongly demanded.

Optical reflectivity $R(\omega)$, bridging the gap separating DC transport properties (or low-frequency spectroscopy) and high-frequency (high-energy) spectroscopy, is a powerful tool for investigating the electrical properties of conducting carriers as well as the electronic structure near the Fermi level [20]. Contrary to the reports of earlier optical studies [21–25] in which the energy $\hbar\omega$ and/or the composition x ranges were limited, this study presents the systematic optical spectra that cover the far-infrared (far-IR) to vacuum-ultraviolet (VUV) frequency range and the insulating to metallic compositional range. This study enabled us to discuss overall electronic states and structures developed by Y doping. Particularly, analyzing *optical conductivity* $\sigma(\omega)$ in the far-IR to near-IR region is fundamentally important to elucidate the valence transition and charge dynamics.

Results presented herein clarified the role of electrons doped onto the 5*d* conduction band by Y dopants to the valence transition. They revealed a marked difference in the valence transition process between that by doping and that by pressure. The doped 5*d* electrons produce the anomalous intermediate metallic state before reaching the valence transition. The Fermi level is shifted upwards because of electron doping in the 5*d* band. Therefore, the valence transition requires a deeper overlap of the 5*d* and 4*f* states in the doping case. This overlap can explain the higher operating temperature of NTE in the doped system than in the pressure-induced case. These results also provide a material-oriented strategy to achieve higher operating temperatures of NTE.

II. EXPERIMENTS

Single crystals of $Sm_{1-x}Y_xS$ were grown using the Bridgeman method [17]. We analyzed the compositional ratio between samarium and yttrium using the inductively coupled plasma atomic emission spectroscopy (ICP-AES) method. The obtained crystals were identified as the monosulfide based on x-ray powder diffraction measurements at room temperature ($T = 295$ K) using Cu $K\alpha$ radiation (Rint2100; Rigaku Corp.). Electrical resistivity $\rho(T)$ was measured using a

*yokoyama@nuap.nagoya-u.ac.jp

conventional four-probe method (2182; Keithley Instruments, Inc.).

Normal incident reflectivity measurements were taken of the cleaved surfaces at 295 K using a Fourier-type interferometer (0.005–1.6 eV, DA-8; ABB Bomem) and a grating spectrometer (1–3 eV, CT25TP; Jasco) installed with a microscope [26]. As a reference mirror, we used an evaporated Au (far- to near-IR region) or Ag (near-IR to visible region) film on a glass plate. We also used synchrotron radiation for the measurements at visible to VUV region (2–30 eV) at the Institute for Molecular Science, Okazaki National Research Institutes (BL7B). The experimental error for the reflectivity ΔR, as determined from the reproducibility, was less than 2% in the present experiments. We took great care to avoid scratching the sample surface even slightly because the material is highly sensitive to scratches [27]. Fresh cleaved surfaces were always used for optical measurements. The cleaved surface was verified as uniform using microscopic observation (Supplemental Material Fig. S1 [28]). In addition, the spectrum is not place dependent within our spatial resolution (approximately 100 μm) for the IR to visible region.

For quantitative discussion, we deduced the optical conductivity $\sigma(\omega)$ from the measured reflectivity $R(\omega)$ via Kramers-Kronig transformation. Optical conductivity $\sigma(\omega)$ is the real part of complex conductivity. It is related to the imaginary part of the dielectric function $\varepsilon_2(\omega)$ in the manner of $\sigma(\omega) = (\omega/4\pi)\varepsilon_2(\omega)$. To use this transformation, appropriate extrapolations are necessary. Because the experiment covers the energy region up to $\hbar\omega = 30$ eV, which includes contributions from most of the valence electrons in the material, our extrapolation to the higher energy region (we assumed $R \propto \omega^{-4}$) does not affect $\sigma(\omega)$ in the energy region of interest. Below 5 meV we made extrapolation by assuming Hagen-Rubens (HR) reflectivity. Parameters in the HR extrapolations $\sigma(0)_{\rm HR}$ are 70 $\Omega^{-1}\,{\rm cm}^{-1}$ ($x = 0$), 2000 $\Omega^{-1}\,{\rm cm}^{-1}$ ($x = 0.10$), 13,000 $\Omega^{-1}\,{\rm cm}^{-1}$ ($x = 0.20$), and 15,000 $\Omega^{-1}\,{\rm cm}^{-1}$ ($x = 0.28$), which are somewhat larger than the measured DC conductivity $\sigma_{\rm DC}$ (39, 1,170, 5470, and 7490 $\Omega^{-1}\,{\rm cm}^{-1}$, respectively, for $x = 0$, 0.10, 0.20, and 0.28), but roughly in accord with the $\sigma_{\rm DC}$ value of the earlier report (approximately 10,000 $\Omega^{-1}\,{\rm cm}^{-1}$ for $x = 0.32$ [29]). In any case, within the range of $\sigma(0)_{\rm HR}$ described above, variation of the HR extrapolation procedures was found to have negligible effects on $\sigma(\omega)$ for values greater than 10 meV (Supplemental Material Fig. S2 [28]).

III. RESULTS

Figure 1 shows the optical reflectivity $R(\omega)$ spectra of $Sm_{1-x}Y_xS$ at room temperature (295 K) on a logarithmic scale (0.001–25 eV). Figure 2 shows the optical conductivity $\sigma(\omega)$ spectra deduced from $R(\omega)$ on a linear scale: (a) 0–1 eV and (b) 0–6 eV.

Many optical studies of SmS have been reported [12,15,27,30–35]. The present spectra of SmS are consistent with those earlier results. The optical response consists of three parts: (1) response from phonons and residual carriers (<1 eV), (2) excitations from Sm^{2+} $4f$ to $5d$ states (0.5–6 eV), and (3) excitations involving S $3p$ and $3s$ states (over 4 eV). The IR spectrum of SmS is characterized by

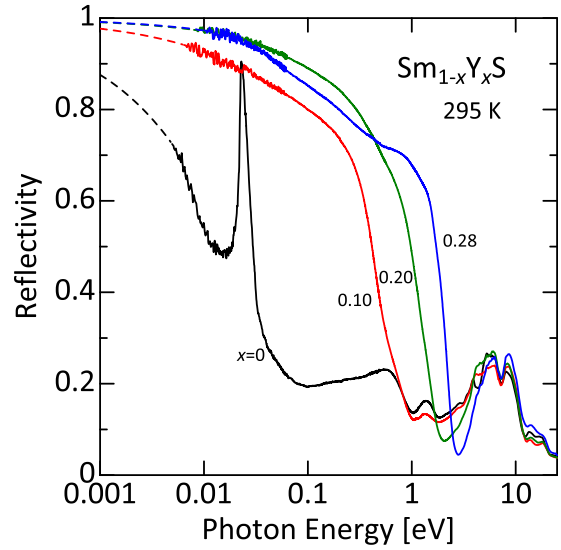

FIG. 1. Optical reflectivity spectra of $Sm_{1-x}Y_xS$ at 295 K up to 25 eV. The dotted line shows the Hagen-Rubens extrapolations. Y doping produces a sharp reflectivity edge. As doping proceeds, the edge shifts to higher energy. Also, reflectivity below the edge becomes higher. At $x = 0.28$, a characteristic structure appears in the reflectivity below the edge.

a pronounced peak at 23 meV and low reflectivity, which is the typical behavior of an insulator. The peak is assigned to a TO phonon of stretching mode. The low reflectivity indicates almost no conducting carriers. As a result, $\sigma(\omega)$ has no remarkable structure other than the TO phonon. The value of $\sigma(\omega)$ is as low as about 70 $\Omega^{-1}\,{\rm cm}^{-1}$, except for the phonon. The spectral weight is also slight. Instead of a Drude peak, the spectrum is characterized by a gap of 0.4 eV, which is consistent with the semiconducting DC conductivity of this material [inset of Fig. 2(a)]. We refer to an additional peak at 8 eV. This peak is not predicted by band calculations [36–38], but careful observation can reveal its presence from earlier spectroscopic experiments [39–41]. A representative reflectivity study [30] also presents a sign, although not as clear as found in this study. The high-energy spectroscopy attributes it to that about 10% of Sm^{3+} exists even in the pure SmS [40].

Next, we examine variation of the spectra by Y doping. A sharp rise appears in $R(\omega)$ by Y doping, which moves to higher energy as the doping proceeds (Fig. 1). The reflectivity edge appears at 1.0, 1.8, and 2.6 eV, respectively, for $x = 0.10$, 0.20, and 0.28. The reflectivity becomes high below the edge. This phenomenon can be regarded as a plasma edge by the electrons doped onto the $5d$ conduction band by Y. It is noteworthy that for $x = 0.28$ the reflectivity exhibits complex energy dependence. It rises once at 2.6 eV, but does not monotonically increase concomitantly with decreasing $\hbar\omega$. Instead, a kink or shoulderlike structure appears at around 0.6 eV. This formation contrasts starkly to the reflectivity spectra of $x = 0.10$ and 0.20, in which $R(\omega)$ increases monotonically with decreasing $\hbar\omega$ below the edge. Furthermore, in the lower-energy region around 0.02 eV, $R(\omega)$ of $x = 0.28$ again becomes slightly higher than that of $x = 0.20$. For the higher-energy region, however, as the doping proceeds, the interband transitions at 1–6 eV observed in SmS become less

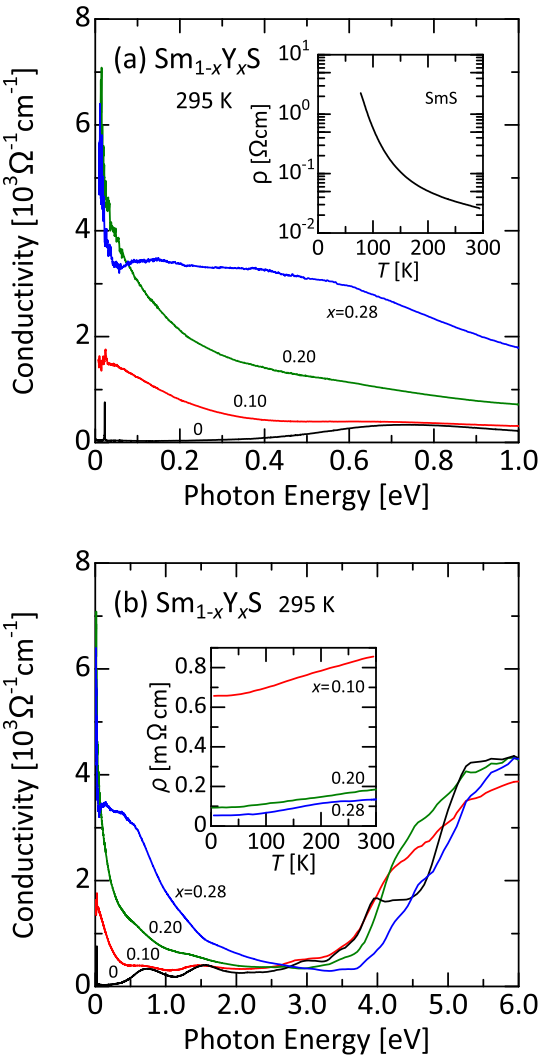

FIG. 2. Optical conductivity spectra of $Sm_{1-x}Y_xS$ at 295 K: (a) 0–1 eV and (b) 0–6 eV. Spectra were deduced by Kramers-Kronig transformation. Insets show the electrical resistivity of $Sm_{1-x}Y_xS$ single crystal. The isosbestic point appears at 2.7 eV. Although the spectral weight in the lower-energy region increases as doping proceeds, it does not obey the simple Drude response. Instead, the prominent mid-IR absorption grows.

clear because they are buried in the low-energy spectrum, which develops as doping proceeds, but the characteristic structure consisting of multiple peaks derived from the interband transitions is maintained.

In optical conductivity $\sigma(\omega)$ spectra, an isosbestic point appears around 2.7 eV. As doping proceeds, the spectral weight of 2.7–6 eV is reduced and moves to 2.7 eV or less [Fig. 2(b)]. This reduction corresponds to the fact that the plasma edge moves to the higher energies. The Y doping immediately changes the system into a metallic one in the sense that the resistivity $\rho(T)$ shows a positive slope ($d\rho/dT > 0$) [29]. However, the optical conductivity in the IR region, which is related directly to electrical conduction, is not simple. For $x = 0.10$ and 0.20, the IR optical conductivity is not characterized by a simple Drude response of $\sigma(\omega) = \sigma(0)\gamma^2/(\omega^2 + \gamma^2)$ with ω^{-2} decay. Here γ is the relaxation rate. Instead,

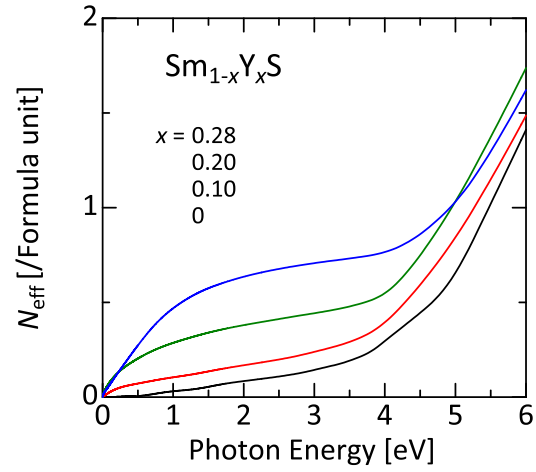

FIG. 3. Integrated spectral weight of $Sm_{1-x}Y_xS$ at 295 K below 6 eV. Intensity near zero energy related directly to the DC conductivity does not increase monotonically, but rather decreases for $x = 0.28$, instead drastically increasing the intensity of the mid-infrared region.

it decays more slowly (typically $\propto\omega^{-1}$). For $x = 0.28$, the zero-frequency peak grows with narrowing of width (less than 50 meV), whereas the spectral weight at mid-IR region around 0.2 eV increases drastically. As a result, the two-component structure shape is clarified. This result corresponds to the characteristic reflectivity described above. Some qualitative change takes place in the charge dynamics around this compositional region. Such reflectivity can be recognized from the past results, although the conductivity was not calculated because $R(\omega)$ was limited at values greater than 0.1 eV [22]. However, the behavior characteristic of $Sm_{1-x}Y_xS$ appears in the far-IR region, especially below 0.1 eV. Particularly the composition dependence of $\sigma(\omega)$ is characterized by a rapid growth below 0.1 eV at $x = 0.28$ in addition to the mid-IR spectral weight. Therefore, reflectivity measurements below 0.1 eV are fundamentally important for conclusive discussion of this point.

The integrated spectral weight defined as

$$N^*_{\rm eff}(\omega) = \frac{2m_0V}{\pi e^2}\int_0^{\omega}\sigma(\omega')d\omega' \qquad (1)$$

(m_0 is the bare-electron mass and V is the unit-cell volume) is portrayed in Fig. 3. Here, as the value of V, the following values obtained from the x-ray diffraction experiments at 295 K [17] were used: $V = 52.95$ Å^3 (x =0), 52.05 Å^3 (x = 0.10), 50.15 Å^3 ($x = 0.20$), and 45.89 Å^3 ($x = 0.28$). The value of $N^*_{\rm eff}(\omega)$ represents the effective density of charges contributing to all optical excitations below a certain cutoff energy $\hbar\omega$ [20,42]. The value of $N^*_{\rm eff}(\omega)$ is defined using bare-electron mass m_0. Therefore, we can discuss effects of mass renormalization using it [15,43]. Higher-energy conductivity is attributable to interband transitions and is unlikely to represent a contribution from the charge carriers. The contribution to the zero-frequency term increases monotonically up to $x = 0.20$, but no longer increases by further doping. $N^*_{\rm eff}(\omega)$ for $x = 0.28$ in the low-energy region is rather slightly smaller than that for $x = 0.20$. Instead, the weight associated

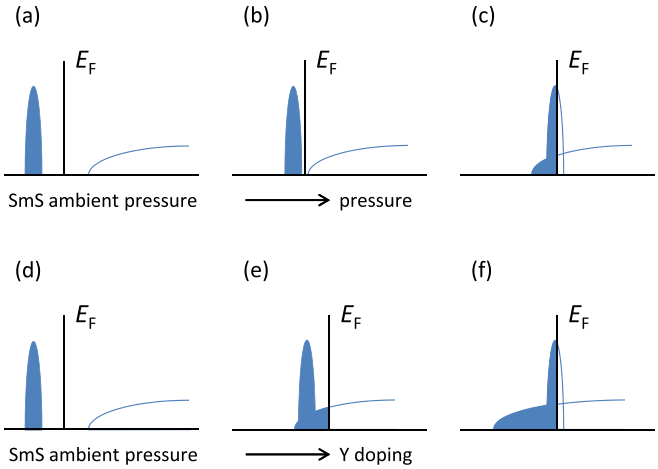

FIG. 4. Schematic diagrams for the electronic structure of SmS developed by (a)–(c) pressure and (d)–(f) doping: (a) and (d) The same electronic state of pure SmS at ambient pressure. In the case of pressure, the valence transition occurs simultaneously with metallization because the system does not become metallic unless the bottom of the "empty" $5d$ band contacts the $4f$ level (b). In the case of doping, the system becomes metallic even though the bottom of the "partially filled" d band does not contact the $4f$ level (e). For the valence transition, the $5d$ band must overlap the weakly dispersive $4f$ band more deeply in the case of doping (f) than in the case of pressure (c).

with the mid-IR absorption increases drastically. Although the spectral weight below 1 eV increases greatly by doping, not all contribute to DC conduction.

IV. DISCUSSION

An earlier report of the literature presents a brief description of the difference between pressure-induced and doping-induced transitions based on the overlap of $4f$ and $5d$ states. Tao and Holtzberg discussed the increase in Fermi energy with Y doping and the similarity between the reentrant Jahn-Teller transition and the reentrant valence transition [8]. Coey *et al.* suggested that the d electrons brought by Y dopants raise the Fermi level and thereby help to stabilize the black phase [44]. Here, based on the characteristic compositional dependence of the measured spectra, we summarize, schematically, the differences in the process of reaching the metallic state between that by pressure and that by doping (Fig. 4). One Y dopant donates one electron onto the $5d$ conduction band [29]. This correspondence differs from the case in which the band gap is collapsed by pressure. In the case of a pressure-induced transition [Figs. 4(a)–4(c)], metallization is expected to accompany the valence transition simultaneously, whereas in the case of doping [Figs. 4(d) and 4(e)], an intermediate metallic phase appears before the valence transition. In earlier studies, the naive picture that electron doping onto the $5d$ band lowers the bottom of the band has been proposed as the origin of the doping-induced valence transition [9]. The bottom of the $5d$ band is lowered only when there exist electrons that can benefit from the energy gain when the band energy is reduced. This is a universal physics in the relation between crystal structure and electronic states. This is fundamentally the same, for example, as the fact that the Jahn-Teller effect depends on the number of electrons. This finding is also similar to the fact that the presence of holes in the Sb $5p$ valence band accelerates p-f mixing effects nonlinearly in CeSb [45]. This difference can explain why Y^{3+} and Nd^{3+} cause valence transition [7] but Ca^{+2} or Yb^{2+} does not, despite having a smaller radius than Sm^{2+} [9]. Definitions of the black and golden phases we often use are actually empirical. They do not accurately reflect the electronic state, such as whether valence transition occurs or not.

A broad zero-frequency peak decaying more slowly than a simple Drude response for $x = 0.10$ and 0.20 suggests an anomalous intermediate metallic state before reaching the valence transition. An anomalous metallic phase has been reported also from earlier studies [7,8,46]. The relation to those results is an interesting future topic. In this compositional range, the $4f$ state remains below the Fermi level and remains fully occupied. Therefore, the charge dynamics is contributed by the $5d$ electrons. Deviation from the simple Drude response indicates that revisiting the $5d$ charge dynamics is worthwhile. Such an unusual response is commonly observed in many strongly correlated systems [42,47–54] including $5d$ systems such as Ir oxides [55]. The close resemblance to those d-electron systems suggests strongly that the charge dynamics for $x = 0.10$ and 0.20 should be discussed in relation to the arguments on those other strongly correlated systems. In any case, the anomalous charge dynamics in these systems are interpreted as suggesting correlated and/or localization characteristics of the carriers [20]. The localized characteristics of the doped $5d$ electrons are suggested in the earlier Mössbauer study [44].

One interpretation is the idea that the relaxation rate has characteristic frequency dependence, for example, $\gamma \propto \omega$, because of interaction between the d electrons and/or interaction with $4f$ states (one-component picture). This picture was proposed by Varma as a *marginal Fermi liquid* concept [56] and was examined using generalized Drude analysis [57] of reflectivity measured on correlated systems such as a high-temperature superconductor $YBa_2Cu_3O_7$ [47] and colossal magnetoresistive $La_{1-x}Sr_xMnO_3$ [53]. Another interpretation is the idea that a small Drude term is actually included in the slowly decayed zero-energy peak. However, even in that case, a huge absorption band in far-IR to near-IR region certainly exists, which has not been described to date (two-component picture). In the case of $Sm_{1-x}Y_xS$, the $4f$ states that approach the Fermi level by Y doping [58] seem to play an important role.

For $x = 0.28$, unlike $x = 0.10$ and 0.20, although the zero-frequency peak grows sharply, the growth in the mid-IR to near-IR region is much larger. Most of the low-energy spectral weight increased by doping is condensed in the mid-IR to near-IR region. Linear thermal expansion measurement [17] revealed discontinuous change in the lattice volume between $x = 0.20$ and $x = 0.28$, suggesting that valence transition occurs in this compositional region. The infrared spectrum for $x = 0.28$ is characteristic of the charge dynamics of the system in which the Fermi level exists within the $4f$ states.

Electrons doped onto the $5d$ band by Y might strongly influence NTE in this system. In the case of pressure-induced transition, the $5d$ band is originally empty. Therefore, even if the bottom of the $5d$ band does not touch the $4f$ level

in the ground state, electrons are easily excited thermally to the $5d$ band. Consequently, the system shifts from Sm^{2+} to Sm^{3+} even at relatively low temperatures where the electrons are not thermally excited to the $5d$ band so much. However, if "nonthermally excited" carriers exist in the $5d$ band by Y doping, the Fermi level is lifted upwards [7,8,44,59]. Valence transition requires that the Fermi level exists within the weakly dispersive $4f$ band and, therefore, the $5d$ band must overlap the $4f$ band more deeply than the pressure-induced case for valence transition. This overlap can explain the higher operating temperature of NTE in the doped system. In fact, NTE is maintained above room temperature in the Y-doped system [17], but it is at the highest 200 K in the pressure-induced case [60]. This scheme can also explain the x-T phase diagram of $Sm_{1-x}Y_xS$ proposed by Tao and Holtzberg [8], in which the M (Sm^{3+}) phase appears abruptly around $x = 0.2$ and the upper limit is as high as about 600 K. The higher operating temperature of NTE is strongly desired from an engineering perspective [16]. Whereas reports of earlier studies have described the volume change and thermal expansion anomaly associated with the valence transition from the viewpoint of fundamental physics [6–8,11,46,61,62], the results of this study demonstrate that the overlap of $5d$ and $4f$ state determines the function of NTE, and especially the upper limit of operating temperature, providing a strategy that an increase of the operating temperature might be achieved by more electron doping, for example, by sulfur deficiency.

The picture by which the $5d$ band penetrates deeper into the weakly dispersive $4f$ band in the Y-doped system might be verified, for example, by detailed observation of the compositional dependence of the excitations at 13–14 eV and 16–17 eV, which are interpreted respectively as S $3s \rightarrow$ Sm $5d(t_{2g})$ and S $3s \rightarrow$ Sm $5d(e_g)$. More-detailed evaluations of the temperature and compositional dependence of the higher-energy electronic structure must be undertaken in future studies.

Timescale of the valence fluctuations is a central concern of SmS research. The earlier Mössbauer study [44] portrays a sharp increase in isomer shift without increase in linewidth by pressure and Y doping. However, the well-defined peak splitting corresponding to Sm^{2+} and Sm^{3+} states are observed from results of x-ray absorption spectroscopy (XAS) [11]. These results suggest that the timescale of the fluctuation falls within the range of 10^{-9}–10^{-15} s. Infrared light is regarded as within the range above, near the upper limit (1 eV corresponding to 2.4×10^{14} Hz). The dramatic change in the optical conductivity according to the doping level and the anomalous charge dynamics might be interpreted as characteristics of the fluctuations rather than a well-defined Sm^{2+} and Sm^{3+} picture supported by XAS. On the other hand, a characteristic structure consisting of multiple peaks in the VUV region derived from the interband transitions seems to remain in shape. This duality of the optical spectra might reflect the time-dependent valence fluctuations. Infrared spectroscopy might be an effective probe for the longstanding problem in this field, timescale of the fluctuations. The recent Mössbauer spectroscopy using synchrotron radiation reported that timescale of Sm valence fluctuations has been successfully detected experimentally in $SmOs_4Sb_{12}$ [63]. Understanding of this problem is expected to progress in the future by combining various spectroscopies.

Lastly, we refer to inhomogeneity at the atomic level that is unavoidable no matter how high the quality of crystals we formed. First, we emphasize that it is by no means divided into SmS and YS domains. In our single crystals, Sm and Y atoms are dispersed uniformly, as evidenced by results obtained from x-ray diffraction experiments (Supplemental Material Fig. S3 [18,28]) and from SEM-EDX analysis [18]. In the case of $Sm_{1-x}Y_xS$, such residual inhomogeneity at the atomic level might be manifested in macroscopic physical properties such as thermal expansion through differences in the atomic radius of Sm [17]. Nevertheless, it is not a simple matter to ascertain how charge carriers behave in such a system. Nonuniformity might not occur in charge dynamics, partly because the atomic scale (approximately 1 Å) is much less than the wavelength of the incident electromagnetic wave (approximately 1000 Å). As related to the case of $Sm_{1-x}Y_xS$, nanoscale phase separation (called *electronic phase separation*) has been discussed in chemically homogeneous manganese oxides [64]. Even in such systems, electronic states have been discussed based on optical spectra measured on bulk samples [65]. Nanoscale phase separation is an important topic for these sulfides also in terms of NTE properties [17]. The present $\sigma(\omega)$ is expected to be useful to support future studies.

V. SUMMARY

We have presented optical spectra of $Sm_{1-x}Y_xS$ single crystals over wide compositional and energy ranges. Unlike the valence transition attributable to pressure, the Y-doped $5d$ electrons produce an anomalous intermediate metallic state, which deviates from the simple Drude response, before reaching the valence transition. We have successfully detected the dramatic change in the optical conductivity spectra in response to the valence transition, which provides us with a valuable research field of Sm valence transition. The presence of $5d$ electrons donated by Y dopants is believed to be responsible for the appearance of NTE from higher temperatures in the Y-doped systems than in the pressure-induced case. Results of the present optical study indicate the importance of sulfur deficiency for improving the operating temperature of giant negative thermal expansion in this system.

ACKNOWLEDGMENTS

The authors are grateful to K. Tanaka, N. Kondo, and E. Nakamura for skillful technical assistance in using vacuum ultraviolet radiation. They also would like thank K. Imura and N. K. Sato for fruitful discussion and R. Kaizu and Y. Yamazaki for their assistance with experiments. This work was partly supported by JSPS KAKENHI Grants No. JP17H02763, No. JP18K19019, and No. JP19H05625 from MEXT, Japan. This work was supported by the NIMS Joint Research Hub Program and was conducted partly at the Materials Design and Characterization Laboratory under the Visiting Researcher Program of the Institute for Solid State Physics, The University of Tokyo. This work was performed at BL7B of UVSOR Synchrotron Facility with the approval of Institute for Molecular Science (IMS), NINS (Proposal No. 30-876).

[1] C. M. Varma, Rev. Mod. Phys. **48**, 219 (1976).
[2] J. M. Lawrence, P. S. Riseborough, and R. D. Parks, Rep. Prog. Phys. **44**, 1 (1981).
[3] A. Sousanis, P. F. Smet, and D. Poelman, Materials **10**, 953 (2017).
[4] R. Higashinaka, A. Yamada, T. D. Matsuda, and Y. Aoki, AIP Adv. **8**, 125017 (2018).
[5] A. Jayaraman, V. Narayanamurti, E. Bucher, and R. G. Maines, Phys. Rev. Lett. **25**, 1430 (1970).
[6] T. Penney and F. Holtzberg, Phys. Rev. Lett. **34**, 322 (1975).
[7] A. Jayaraman, P. Dernier, and L. D. Longinotti, Phys. Rev. B **11**, 2783 (1975).
[8] L. J. Tao and F. Holtzberg, Phys. Rev. B **11**, 3842 (1975).
[9] A. Jayaraman and R. G. Maines, Phys. Rev. B **19**, 4154 (1979).
[10] P. P. Deen, D. Braithwaite, N. Kernavanois, L. Paolasini, S. Raymond, A. Barla, G. Lapertot, and J. P. Sanchez, Phys. Rev. B **71**, 245118 (2005).
[11] P. A. Alekseev, J.-M. Mignot, E. V. Nefeodova, K. S. Nemkovski, V. N. Lazukov, N. N. Tiden, A. P. Menushenkov, R. V. Chernikov, K. V. Klementiev, A. Ochiai, A. V. Golubkov, R. I. Bewley, A. V. Rybina, and I. P. Sadikov, Phys. Rev. B **74**, 035114 (2006).
[12] K. Matsubayashi, K. Imura, H. S. Suzuki, T. Mizuno, S. Kimura, T. Nishioka, K. Kodama, and N. K. Sato, J. Phys. Soc. Jpn. **76**, 064601 (2007).
[13] H. Takahashi, R. Okazaki, H. Taniguchi, I. Terasaki, M. Saito, K. Imura, K. Deguchi, N. K. Sato, and H. S. Suzuki, Phys. Rev. B **89**, 195103 (2014).
[14] P. Wachter, A. Jung, and F. Pfuner, Phys. Lett. A **359**, 528 (2006).
[15] T. Mizuno, T. Izuka, S. Kimura, K. Matsubayashi, K. Imura, H. S. Suzuki, and N. K. Sato, J. Phys. Soc. Jpn. **77**, 113704 (2008).
[16] K. Takenaka, Front. Chem. **6**, 267 (2018).
[17] K. Takenaka, D. Asai, R. Kaizu, Y. Mizuno, Y. Yokoyama, Y. Okamoto, N. Katayama, H. S. Suzuki, and Y. Imanaka, Sci. Rep. **9**, 122 (2019).
[18] D. Asai, Y. Mizuno, H. Hasegawa, Y. Yokoyama, Y. Okamoto, N. Katayama, H. S. Suzuki, Y. Imanaka, and K. Takenaka, Appl. Phys. Lett. **114**, 141902 (2019).
[19] D. G. Mazzone, M. Dzero, M. Abeykoon, H. Yamaoka, H. Ishii, N. Hiraoka, J. P. Rueff, J. Ablett, K. Imura, H. S. Suzuki, J. N. Hancock, and I. Jarrige, arXiv:1905.03090.
[20] D. N. Basov, R. D. Averitt, D. van der Marel, M. Dressel, and K. Haule, Rev. Mod. Phys. **83**, 471 (2011).
[21] G. Güntherodt and F. Holtzberg, AIP Conf. Proc. **24**, 36 (1975).
[22] G. Güntherodt and F. Holtzberg, Solid State Commun. **18**, 181 (1976).
[23] G. Güntherodt, A. Jayaraman, E. Anastassakis, E. Bucher, and H. Bach, Phys. Rev. Lett. **46**, 855 (1981).
[24] S. N. G. Corder, X. Z. Chen, S. Q. Zhang, F. R. Hu, J. W. Zhang, Y. L. Luan, J. A. Logan, T. Ciavatti, H. A. Bechtel, M. C. Martin, M. Aronson, H. S. Suzuki, S. Kimura, T. Iizuka, Z. Fei, K. Imura, N. K. Sato, T. H. Tao, and M. K. Liu, Nat. Commun. **8**, 2262 (2017).
[25] R. Ikeda, H. Watanabe, Y. Negoro, Y. Takeno, K. Imura, H. S. Suzuki, N. K. Sato, and S. Kimura, J. Phys.: Conf. Ser. **1220**, 012005 (2019).
[26] K. Takenaka, S. Kashima, A. Osuka, S. Sugai, Y. Yasui, S. Shamoto, and M. Sato, Phys. Rev. B **63**, 115113 (2001).
[27] B. Batlogg, E. Kaldis, A. Schlegel, and P. Wachter, Phys. Rev. B **14**, 5503 (1976).
[28] See Supplemental Material at http://link.aps.org/supplemental/10.1103/PhysRevB.100.245143 for microscopic observation images, optical conductivity calculated with several kinds of Hagen-Rubens (HR) extrapolation, and x-ray diffraction results.
[29] K. Imura, M. Saito, M. Kaneko, T. Ito, T. Hajiri, M. Matsunami, S. Kimura, K. Deguchi, H. S. Suzuki, and N. K. Sato, J. Phys.: Conf. Ser. **592**, 012028 (2015).
[30] G. Güntherodt, J. L. Freeouf, and F. Holtzberg, Solid State Commun. **47**, 677 (1983).
[31] B. Hillebrands and G. Güntherodt, Solid State Commun. **47**, 681 (1983).
[32] G. Travaglini and P. Wachter, Phys. Rev. B **30**, 5877 (1984).
[33] V. Zelezny, J. Petzelt, V. V. Kaminski, M. V. Romanova, and A. V. Golubkov, Solid State Commun. **72**, 43 (1989).
[34] S. Kimura, T. Mizuno, K. Matsubayashi, K. Imura, H. S. Suzuki, and N. K. Sato, Physica B **403**, 805 (2008).
[35] E. Rogers, P. F. Smet, P. Dorenbos, D. Poelman, and E. van der Kolk, J. Phys.: Condens. Matter **22**, 015005 (2010).
[36] C. Lehner, M. Richter, and H. Eschrig, Phys. Rev. B **58**, 6807 (1998).
[37] V. N. Antonov, B. N. Harmon, and A. N. Yaresko, Phys. Rev. B **66**, 165208 (2002).
[38] A. Svane, V. Kanchana, G. Vaitheeswaran, G. Santi, W. M. Temmerman, Z. Szotek, P. Strange, and L. Petit, Phys. Rev. B **71**, 045119 (2005).
[39] M. Campagna, E. Bucher, G. K. Wertheim, and L. D. Longinotti, Phys. Rev. Lett. **33**, 165 (1974).
[40] A. Chainani, H. Kumigashira, T. Ito, T. Sato, T. Takahashi, T. Yokoya, T. Higuchi, T. Takeuchi, S. Shin, and N. K. Sato, Phys. Rev. B **65**, 155201 (2002).
[41] V. N. Antonov, L. V. Bekenov, and A. N. Yaresko, Adv. Condens. Mater. Phys. **2011**, 298928 (2011).
[42] S. Uchida, T. Ido, H. Takagi, T. Arima, Y. Tokura, and S. Tajima, Phys. Rev. B **43**, 7942 (1991).
[43] J. T. Devreese, L. F. Lemmens, and J. Van Royen, Phys. Rev. B **15**, 1212 (1977).
[44] J. M. D. Coey, S. K. Ghatak, M. Avignon, and F. Holtzberg, Phys. Rev. B **14**, 3744 (1976).
[45] H. Takahashi and T. Kasuya, J. Phys. C: Solid State Phys. **18**, 2697 (1985).
[46] H. A. Mook, R. M. Nicklow, T. Penney, F. Holtzberg, and M. W. Shafer, Phys. Rev. B **18**, 2925 (1978).
[47] Z. Schlesinger, R. T. Collins, F. Holtzberg, C. Feild, G. Koren, and A. Gupta, Phys. Rev. B **41**, 11237 (1990).
[48] P. Kostic, Y. Okada, N. C. Collins, Z. Schlesinger, J. W. Reiner, L. Klein, A. Kapitulnik, T. H. Geballe, and M. R. Beasley, Phys. Rev. Lett. **81**, 2498 (1998).
[49] T. Katsufuji and Y. Tokura, Phys. Rev. B **60**, 7673 (1999).
[50] K. Takenaka, Y. Sawaki, R. Shiozaki, and S. Sugai, Phys. Rev. B **62**, 13864 (2000).
[51] Y. S. Lee, J. Yu, J. S. Lee, T. W. Noh, T.-H. Gimm, H.-Y. Choi, and C. B. Eom, Phys. Rev. B **66**, 041104(R) (2002).
[52] K. Takenaka, R. Shiozaki, S. Okuyama, J. Nohara, A. Osuka, Y. Takayanagi, and S. Sugai, Phys. Rev. B **65**, 092405 (2002).
[53] K. Takenaka, R. Shiozaki, and S. Sugai, Phys. Rev. B **65**, 184436 (2002).

[54] P. E. Jönsson, K. Takenaka, S. Niitaka, T. Sasagawa, S. Sugai, and H. Takagi, Phys. Rev. Lett. **99**, 167402 (2007).

[55] K. Ueda, J. Fujioka, Y. Takahashi, T. Suzuki, S. Ishiwata, Y. Taguchi, and Y. Tokura, Phys. Rev. Lett. **109**, 136402 (2012).

[56] C. M. Varma, P. B. Littlewood, S. Schmitt-Rink, E. Abrahams, and A. E. Ruckenstein, Phys. Rev. Lett. **63**, 1996 (1989).

[57] B. C. Webb, A. J. Sievers, and T. Mihalisin, Phys. Rev. Lett. **57**, 1951 (1986).

[58] K. Imura, T. Hajiri, M. Matsunami, S. Kimura, M. Kaneko, T. Ito, Y. Nishi, N. K. Sato, and H. S. Suziki, J. Korean Phys. Soc. **62**, 2028 (2013).

[59] J. L. Freeouf, D. E. Eastman, W. D. Grobman, F. Holtzberg, and J. B. Torrance, Phys. Rev. Lett. **33**, 161 (1974).

[60] K. Matsubayashi, K. Imura, H. S. Suzuki, G. Chen, N. Mori, T. Nishioka, K. Deguchi, and N. K. Sato, J. Phys. Soc. Jpn. **76**, 033602 (2007).

[61] S. von Molnar and F. Holtzberg, AIP Conf. Proc. **29**, 394 (1976).

[62] H. Bilz, G. Güntherodt, W. Kleppmann, and W. Kress, Phys. Rev. Lett. **43**, 1998 (1979).

[63] S. Tsutsui, J. Nakamura, Y. Kobayashi, Y. Yoda, M. Mizumaki, A. Yamada, R. Higashinaka, T. D. Matsuda, and Y. Aoki, J. Phys. Soc. Jpn. **88**, 023701 (2019).

[64] S. Yunoki, J. Hu, A. L. Malvezzi, A. Moreo, N. Furukawa, and E. Dagotto, Phys. Rev. Lett. **80**, 845 (1998).

[65] A. K. Sarychev, S. O. Boyarintsev, A. L. Rakhmanov, K. I. Kugel, and Yu. P. Sukhorukov, Phys. Rev. Lett. **107**, 267401 (2011).